AGU PUBLICATIONS

JGR

Journal of Geophysical Research: Atmospheres

RESEARCH ARTICLE
10.1002/2014JD022293

Key Points:
- Land surface albedo increase preferentially cools hot extremes by two mechanisms
- Enhanced albedo leads to a reduction of soil moisture drying in midlatitudes
- Cooling intensity projected to increase with climate change in the 21st century

Supporting Information:
- Readme
- Text S1
- Figure S1
- Figure S2

Correspondence to:
M. Wilhelm,
micah.wilhelm@env.ethz.ch

Citation:
Wilhelm, M., E. L. Davin, and S. I. Seneviratne (2015), Climate engineering of vegetated land for hot extremes mitigation: An Earth system model sensitivity study, *J. Geophys. Res. Atmos.*, *120*, 2612–2623, doi:10.1002/2014JD022293.

Received 8 JUL 2014
Accepted 26 FEB 2015
Accepted article online 2 MAR 2015
Published online 1 APR 2015

Climate engineering of vegetated land for hot extremes mitigation: An Earth system model sensitivity study

Micah Wilhelm[1], Edouard L. Davin[1], and Sonia I. Seneviratne[1]

[1]Institute for Atmospheric and Climate Science, ETH Zurich, Zurich, Switzerland

Abstract Various climate engineering schemes have been proposed as a way to curb anthropogenic climate change. Land climate engineering schemes aiming to reduce the amount of solar radiation absorbed at the surface by changes in land surface albedo have been considered in a limited number of investigations. However, global studies on this topic have generally focused on the impacts on mean climate rather than extremes. Here we present the results of a series of transient global climate engineering sensitivity experiments performed with the Community Earth System Model over the time period 1950–2100 under historical and Representative Concentration Pathway 8.5 scenarios. Four sets of experiments are performed in which the surface albedo over snow-free vegetated grid points is increased respectively by 0.05, 0.10, 0.15, and 0.20. The simulations show a preferential cooling of hot extremes relative to mean temperatures throughout the Northern midlatitudes during boreal summer under the late twentieth century conditions. Two main mechanisms drive this response: On the one hand, a stronger efficacy of the albedo-induced radiative forcing on days with high incoming shortwave radiation and, on the other hand, enhanced soil moisture-induced evaporative cooling during the warmest days relative to the control simulation due to accumulated soil moisture storage and reduced drying. The latter effect is dominant in summer in midlatitude regions and also implies a reduction of summer drought conditions. It thus constitutes another important benefit of surface albedo modifications in reducing climate change impacts. The simulated response for the end of the 21st century conditions is of the same sign as that for the end of the twentieth century conditions but indicates an increasing absolute impact of land surface albedo increases in reducing mean and extreme temperatures under enhanced greenhouse gas forcing.

1. Introduction

Mitigation efforts to reduce anthropogenic greenhouse gas emissions have thus far proven inadequate, as evidenced by accelerating CO_2 emissions [*Friedlingstein et al.*, 2014], and the cumulative anthropogenic radiative forcing realized since the industrial revolution is likely to be irreversible on a millennial time scale [*Weaver et al.*, 2007; *Solomon et al.*, 2009]. Moreover, there is a consensus that, as a result of such forcing, the frequency of daily hot extremes such as hot days and heat waves are increasing [*Alexander et al.*, 2006; *Donat et al.*, 2013; *Seneviratne et al.*, 2014] and will continue to do so under global warming [*Tebaldi et al.*, 2006; *Orlowsky and Seneviratne*, 2012; *Seneviratne et al.*, 2012; *Intergovernmental Panel on Climate Change* (*IPCC*), 2012; *Sillmann et al.*, 2013; *IPCC*, 2013]. In addition, some subtropical and midlatitude regions are projected to experience more frequent and intense droughts within the next century [*Orlowsky and Seneviratne*, 2012, 2013]. Such climate extremes have major implications for human health, mortality, forest fires, water availability, and agricultural production [*IPCC*, 2012].

In light of these findings, there has been resurgence in the scientific discourse regarding climate engineering schemes to counter anthropogenic radiative forcing [*Wigley*, 2006; *Lenton and Vaughan*, 2009; *Ridgwell et al.*, 2009; *Doughty et al.*, 2011; *Vaughan and Lenton*, 2011; *Irvine et al.*, 2011; *Singarayer and Davies-Barnard*, 2012; *Curry et al.*, 2014; *Davin et al.*, 2014]. Climate engineering (sometimes termed geoengineering) is the direct modification of the Earth's radiation balance to counteract anthropogenic climate change [*Shepherd and Working Group on Geoengineering the Climate*, 2009; *IPCC*, 2013]. Carbon dioxide removal schemes such as afforestation, biochar production, ocean fertilization, and carbon capture-storage seek to decrease the atmospheric concentration of carbon dioxide and thus to reduce the amount of long-wave radiation trapped in the atmosphere [*Lenton and Vaughan*, 2009; *Shepherd and Working Group on Geoengineering the Climate*, 2009; *IPCC*, 2013]. Solar radiation management (SRM) schemes, on the other hand, seek to decrease the absorption of solar radiation at the Earth's surface. Much attention has been paid to large-scale SRM schemes

such as the deployment of orbiting sunshades, the dispersion of stratospheric aerosols, and the emission of cloud condensation nuclei to brighten marine clouds [*IPCC*, 2013]. Modeling studies suggest that sunshades and stratospheric aerosols show high to moderate scalability to substantially offset anthropogenic climate forcing, whereas cloud brightening exhibits less certainty [*IPCC*, 2013]. However, these methods typically have the inherent disadvantage of extensive implementation costs associated with the creation and maintenance of new large-scale infrastructures. Several potential side effects such as stratospheric ozone depletion and degradation of surface air quality and the problem of short efficacy time scales that necessitate continued reapplication have been identified [*Wigley*, 2006; *Lenton and Vaughan*, 2009; *Vaughan and Lenton*, 2011].

Currently, agricultural lands such as cropland and pastures account for approximately 35 to 40% of the global land surface [*Foley et al*., 2005; *Ramankutty et al*., 2008] and are expected to expand in the near future to meet growing food demand. The use of agricultural land for climate engineering has the advantage of existing agricultural infrastructure with which to modify the Earth's surface energy and radiation balances. Management techniques such as conservation tillage, double cropping, planting of plant varieties with highly reflective leaf trichomes as well as crop dusting with waxy compounds can be relatively rapidly implemented and can effectively modify land-atmosphere fluxes and surface climate conditions [*Lobell et al*., 2006; *Ridgwell et al*., 2009; *Doughty et al*., 2011; *Davin et al*., 2014]. All of these techniques can increase albedo, in turn reducing the amount of solar radiation absorbed at the surface. In addition, the surface albedo of forested areas—currently 30 to 35% of the global land surface [*Goldewijk*, 2001]—can also be modified by forest management [*Luyssaert et al*., 2014]. Presently, a large proportion of forested areas, roughly two thirds, is managed by humans [*Bellassen and Luyssaert*, 2014; *Luyssaert et al*., 2014. Overall, this represents a significant fraction of ice-free land area over which humans can deliberately influence surface albedo.

Previous investigations on the impacts of land surface albedo modifications on climate have focused on the mean climate response [*Lobell et al*., 2006; *Oleson et al*., 2010; *Ridgwell et al*., 2009; *Doughty et al*., 2011]. More recently, a regional study for the European continent analyzed the climate response to changes in summer land surface albedo in the context of no-till agriculture (a type of conservation tillage) and found a strong cooling of hot extremes during the summer months relative to mean temperature under present climate conditions [*Davin et al*., 2014, hereinafter D14]. The extrapolation of these results to the global scale under both present and future climate conditions still remains to be addressed and would be of high relevance for climate engineering scenarios.

Moreover, the possible impacts of surface albedo modification on other land surface variables, such as soil moisture, have not been addressed thus far. Soil moisture variations have been shown to be critical in controlling land-atmosphere exchanges and in affecting regional climate in transitional climate regimes (see, e.g., *Seneviratne et al*. [2010] for a review). Increased surface albedo leads to a reduction in absorbed radiation and cooling at the surface, resulting in less evapotranspiration, thus possibly leading to more soil water savings. These would affect temperature [*Koster et al*., 2006] and temperature variability [*Seneviratne et al*., 2006], including extremes [*Fischer et al*., 2007; *Hirschi et al*., 2011; *Mueller and Seneviratne*, 2012; *Seneviratne et al*., 2013; *Miralles et al*., 2014], potentially leading to an additional cooling, which in some cases could be larger than that for mean temperature [*Seneviratne et al*., 2013]. In addition, feedbacks with precipitation may also be possible [*Koster et al*., 2004; *Taylor et al*., 2012a], although these appear less robust and are more debated in the literature [*Koster et al*., 2010; *Seneviratne et al*., 2010; *Guillod et al*., 2014].

Here we investigate the potential for large-scale modifications of the albedo of vegetated areas to mitigate temperature extremes for recent and future (20th and 21st centuries) climate conditions using a fully coupled Earth system model. In addition, we also assess whether yearlong changes in surface albedo lead to a substantially different response in midlatitude summer conditions compared to an albedo modification focused on summer months only (e.g., from no-till agriculture, D14). While the applied modifications are of large geographical extent and thus of mostly a hypothetical nature, they provide an upper bound estimate for the potential effects of climate engineering from changes in land surface albedo (e.g., from double cropping, highly reflective cultivars, crop dusting, conservation tillage, and forest management).

2. Methods

2.1. Model Description

We employ a fully coupled Community Earth System Model (CESM) version 1.0.4, which is composed of five model components simulating the Earth's atmosphere, land, land ice, ocean, and sea ice [*Gent et al*., 2011].

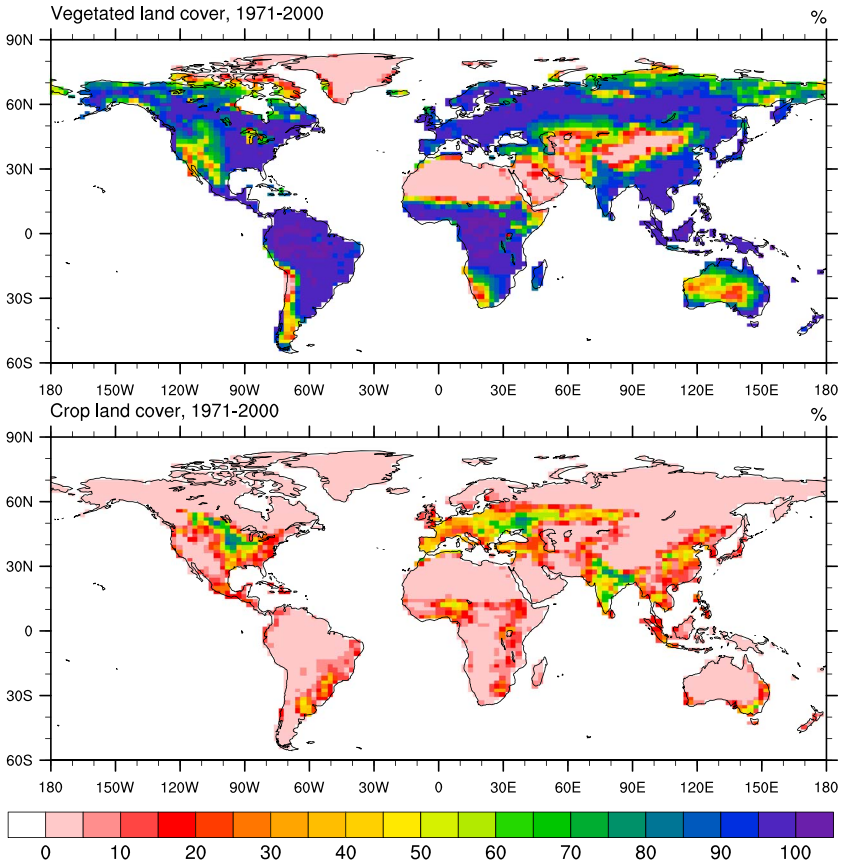

Figure 1. Percentages of total (top) vegetation and (bottom) cropland prescribed in all experiments with CESM. Land cover maps are transient and are therefore displayed over the period 1971–2000 in summer (JJA).

The former three model components are run at a horizontal resolution of 1.9° × 2.5°, while the latter two are run at 1° × 1° on a Greenland-displaced pole grid. The land component, the Community Land Model version 4.0 (CLM4), calculates fluxes of heat, reflected and emitted radiation, momentum, water vapor, carbon, nitrogen, dust, biogenic volatile organic compounds, and other trace gases between the land surface and atmosphere.

CLM4 has a subgrid tiling structure to represent the land units: vegetated, urban, lake, wetland, and glacier. Over the soil columns of each vegetated grid point, differing coverage of 16 plant functional types (PFTs) are transiently prescribed. The PFTs for natural vegetation classes are parameterized with specific optical, biophysical, and aerodynamic properties. There is one PFT that describes a generic crop, which is parameterized identically to C3 grasses. All PFTs are forced with identical atmospheric conditions within the same grid point. All vegetation state variables such as canopy water storage and vegetation temperature are defined for each PFT. Land to atmosphere boundary fluxes and surface variables are weighted by PFT coverage. Prognostic calculations of the carbon and nitrogen cycles are integrated into CLM4's biophysical processes. Carbon pools are translated into various physiological properties such as leaf area index, stem area index, and canopy thickness. Plant phenology is also prognostic and is affected by soil water availability, air and soil temperature, and day length to varying extents for each PFT.

2.2. Simulation Setup

We carry out a control simulation (referred to as CTL) over the time period 1950–2100 corresponding to the setup of the fifth phase of the Coupled Model Intercomparison Project (CMIP5) [*Taylor et al*., 2012b], as well as a series of sensitivity experiments with differing levels of increased surface albedo. In the latter simulations, we apply 0.05, 0.10, 0.15, and 0.20 increases in surface albedo over all snow-free vegetated regions (Figure 1). These sensitivity experiments are referred to as EXP05, EXP10, EXP15, and EXP20, respectively.

Table 1. Experimental Summary

Experiment	Surface Albedo Increase	Over PFT	Time of Increase	CO_2 Scenario
CTL	-	-	-	Historical/RCP8.5
EXP05	0.05	all	all year	Historical/RCP8.5
EXP10	0.10	all	all year	Historical/RCP8.5
EXP15	0.15	all	all year	Historical/RCP8.5
EXP20	0.20	all	all year	Historical/RCP8.5
EXP10c	0.10	crops	all year	Historical/RCP8.5
EXP10cJA	0.10	crops	July and August	Historical/RCP8.5

The surface albedo increases were chosen to bracket a range of possible surface albedo changes achievable though various land management types. For instance, the upper bound for the albedo increase achievable through no-till agriculture is estimated to be around 0.2; though, 0.1 is a more likely value [D14]. Albedo changes on the order of 0.05 are typical values for leaf albedo engineering or forest management [*Singarayer and Davies-Barnard*, 2012; *Luyssaert et al.*, 2014]. It is important to note that the spatial extent of the albedo increase is highly idealized in that it does not take into account current or future agricultural extent.

A simulation identical to EXP10 except that the albedo modification is carried out over cropland only was additionally performed (referred to as EXP10c). This experiment enables us to assess the magnitude of the climate response if the albedo increase is restricted to cropland areas. A further simulation, EXP10cJA, is identical to EXP10c except that the albedo modification is only applied over cropland during the months of July and August. This allows us to investigate the influence of the time period over which the albedo increase is applied. Indeed, land management such as conservation tillage is expected to increase albedo during a limited time period after harvest [D14].

An overview of all performed experiments is provided in Table 1. Each simulation is initialized from the same preexisting historical run at 1950 and is integrated forward in time by 30 min time steps under historical forcing until 2005 followed by Representative Concentration Pathway 8.5 (RCP8.5) forcing until 2100. All analyses presented here are based on daily model output.

2.3. Tmax Percentile Composites

To analyze the climate response to albedo change as a function of daily maximum temperature (Tmax), daily variables of relevance are binned at each grid point according to the Tmax percentiles of the respective simulation in steps of 10%. For each of the resulting 10 bins, the data are averaged in time (June-July-August (JJA)) and space (e.g., over a region of interest). The resulting aggregated values are then used to calculate anomalies (EXP-CTL).

3. Results

3.1. Impact of Albedo Increase on Summer Temperature and Hot Extremes

Surface albedo increase (EXP10) results in a decrease in maximum daily 2 m air temperature (Tmax) in summer over most of the land area (Figure 2a). The strongest cooling effect occurs over vegetated regions above 30°N, while tropical and subtropical regions as well as less densely vegetated areas exhibit a weaker cooling. The cooling of hot extremes (90th percentile of Tmax; henceforth Tmax90) follows a similar spatial pattern but tends to be amplified compared to the decrease in mean Tmax (Figure 2b). The stronger decrease of hot temperatures relative to mean temperatures is hereafter referred to as "preferential cooling." Changes in indices of hot extremes such as the heat wave duration index (HWDI) and the yearly maximum Tmax (TXx) were found to be consistent with changes in Tmax90 in spatial pattern and sign across all four sensitivity experiments (not shown). This implies that the land climate engineering might not only reduce the local intensity of heat waves but may also influence their duration. The effects of surface albedo increases on the aforementioned hot extreme indices as well as the preferential cooling ratio (Tmax90/Tmax) are summarized in Table 2.

The magnitude of the preferential cooling (shown as the absolute difference between the change in Tmax90 and the change in mean Tmax in Figure 2c) is greatest over Central Europe (CEU), central North America (CNA), southern South America, and southern Australia. In these regions, the decrease in Tmax90

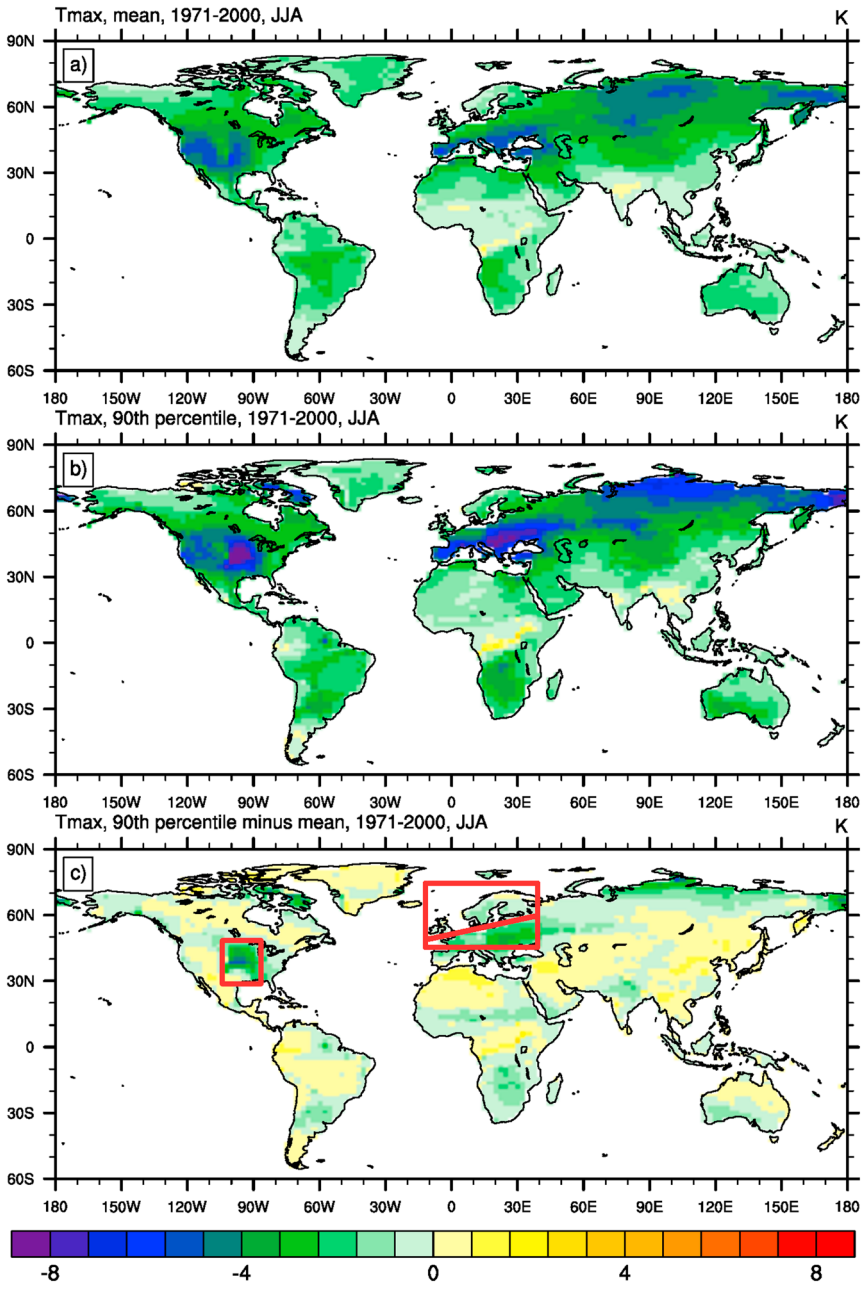

Figure 2. Summer (JJA) change (EXP10 minus CTL) in (a) Tmax (mean daily maximum 2 m air temperature) and (b) the 90th percentile of Tmax for the period 1971–2000. (c) The difference between Figures 2b and 2a as a measure of the magnitude of preferential cooling. The regions NEU, CEU, and CNA defined by *IPCC* [2012] are indicated in red in Figure 2c.

ranges approximately from 120% to 200% that of the mean Tmax. Hence, part of our analyses in the following sections focus on those regions (Northern Europe (NEU), CEU, and CNA) exhibiting the strongest preferential cooling effect.

3.2. Mechanisms and Components of Preferential Cooling

In the following subsections, we analyze the mechanisms contributing to the preferential cooling on a regional scale. We illustrate results over both NEU and CEU (boundaries indicated in Figure 2c), but note that results over CNA are qualitatively similar as those over CEU and are shown in Figure S1 in the supporting information. Figures 3 and 4 provide the basis for the analysis of the underlying processes, whereas Figure 5 summarizes conceptually the identified mechanisms behind the preferential cooling.

Table 2. Changes in Hot Extreme Indices and Preferential Cooling Over Cropland[a]

Experiment	Tmax	Tmax90	Tmax90/Tmax	HWDI	TXx
EXP05-CTL	−3.44	−2.38	1.44	−0.568	−3.19
EXP10-CTL	−6.43	−4.55	1.41	−1.905	−9.55
EXP15-CTL	−8.46	−6.13	1.38	−1.864	−9.59
EXP20-CTL	−10.41	−7.79	1.34	−1.977	−14.97
EXP10c-CTL	−2.96	−1.95	1.52	0.651	−1.06
EXP10cJA-CTL	−1.14	−0.76	1.5	0.029	−2.57

[a]Preferential cooling ratio (90th percentile of Tmax divided by mean Tmax), warm spell duration index (WSDI), heat wave duration index (HWDI), and annual maximum Tmax (TXx) for July and August, 1971–2000 over grid points north of 30°N with vegetation and cropland of 60% or greater.

3.2.1. Asymmetric Radiative Forcing

The changes (EXP10-CTL) of various variables are shown in Figure 3 as a function of Tmax percentiles. Over both NEU and CEU, the albedo-induced increase in reflected solar radiation (SWup) is larger for higher Tmax. This is due to predominantly clear sky conditions during hot days and thus greater downwelling solar radiation (SWdwn), leading to larger solar radiation loss for a given albedo increase, as also highlighted by D14. This asymmetric forcing alone contributes to an amplification of the cooling effect during the hottest days.

However, resulting changes in net shortwave radiation (SWnet = SWdwn − SWup) absorbed at the surface reflect not only changes in surface albedo but also changes in incoming shortwave radiation owing to cloud cover feedbacks (see SWdwn and SWnet in Figure 3). Over CEU, an increase in cloud cover leads to a decrease in SWdwn further reducing net solar radiation. This SWdwn reduction is greatest during colder days and thus counterbalances the initial asymmetric radiative forcing, leading to a constant change in SWnet across the temperature distribution. In contrast, cloud cover and SWdwn changes occur over NEU but without strengthening or dampening the initial asymmetry of the radiative forcing. As a consequence, the asymmetric radiative forcing remains the main factor explaining the preferential cooling for hot extremes over NEU. It should be noted that cloud cover feedbacks are a major source of uncertainty in climate model projections [e.g., *Stevens and Bony*, 2013], and we therefore anticipate that the sign and strength of the cloud cover response and associated radiative feedbacks occurring in our simulations are likely to be highly model dependent.

In summary, the asymmetric radiative forcing mechanism prevails only in northern (energy-limited) regions (see Figure 5a), while cloud feedbacks counterbalance this asymmetric forcing in southern regions (e.g., CEU and CNA). In these regions, soil moisture feedbacks play a more central role.

3.2.2. Soil Moisture Feedback

As discussed in the previous section, the change in SWnet alone cannot account for the preferential cooling of hot temperatures in CEU and CNA.

Following the decrease in SWnet, an overall decrease in both sensible (SH) and latent heat (LH) fluxes occur over CEU (Figure 3). However, a prominent increase in evaporative fraction (EF), defined as the fraction of

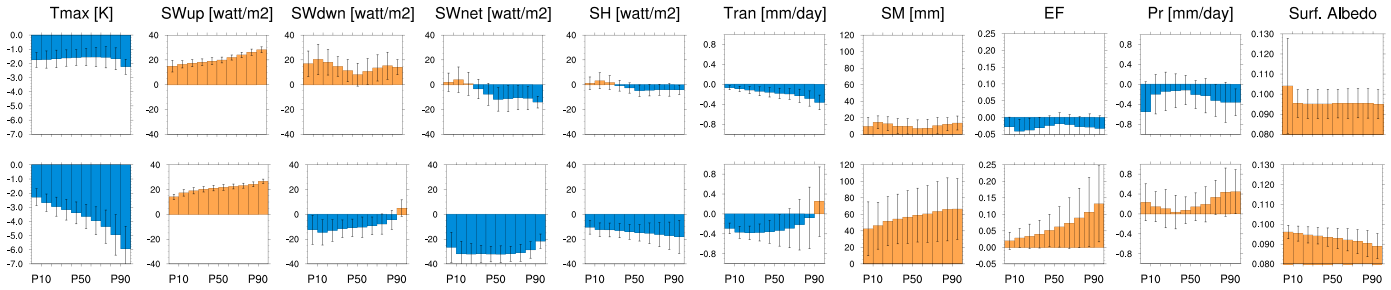

Figure 3. Summer (JJA) change (EXP10 minus CTL) in various variables binned by daily Tmax percentiles for the period 1971–2000 over the regions (top) NEU and (bottom) CEU. Where SW is shortwave radiation, SH is sensible heat flux to the atmosphere, Tran is transpiration, SM is soil moisture, EF is evaporative fraction, and Pr is precipitation. Only grid points with vegetation cover of 60% or greater are taken into account. Error bars indicate the standard deviation of anomalies calculated across all considered grid points.

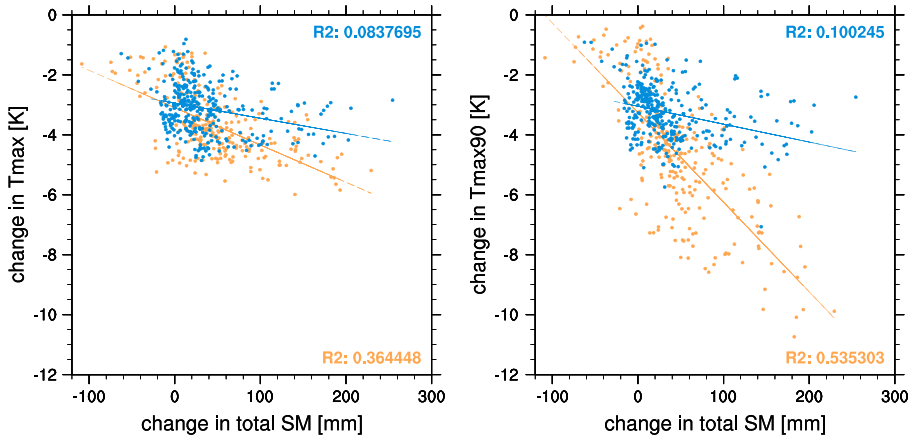

Figure 4. The influence of land cover types and total soil moisture on the change (EXP10 minus CTL) in Tmax and Tmax90 (90th percentile of Tmax) for the period 1971–2000. Only grid points with 60% or greater of grasses and crops (blue) or forests (orange) are considered. The R^2 values of each linear regression are shown.

energy absorbed at the surface contributing to LH, is observed with the maximum occurring during the hottest days. This response is driven by an overall increase in soil moisture (SM) accumulated throughout the year due to the overall evapotranspiration decrease. From the standpoint of evapotranspiration, this soil moisture increase provides a negative feedback, which tends to dampen the initial radiation-induced evapotranspiration decrease. However, this negative feedback, as also noted in D14, is stronger at times of high evaporative demand (i.e., during hot days) even reversing the sign of the evapotranspiration change. This leads to the preferential increase in EF noted above and the preferential cooling of hot extremes.

In line with our expectations, this mechanism involving soil moisture prevails in southern (soil moisture-limited) regions (see Figure 5b). Indeed, both CEU and CNA are situated in a transitional zone between soil moisture and radiation-limited regimes, as indicated by our analysis of the interannual correlation between evapotranspiration (ET) and SWdwn (Figure S2) (see also *Koster et al.* [2004], *Seneviratne et al.* [2006], and *Teuling et al.* [2009]), where soil moisture has more influence on summer temperatures [*Seneviratne et al.*, 2010; *Mueller and Seneviratne*, 2012]. Moreover, in the considered regions the land cover is dominated by grasslands, which have shallow rooting depths. This makes the regions relatively sensitive to a given SM increase during warmer days when the top soil layers might otherwise dry out, thus halting transpiration, while forests may still extract water from deeper layers (see Figure 4).

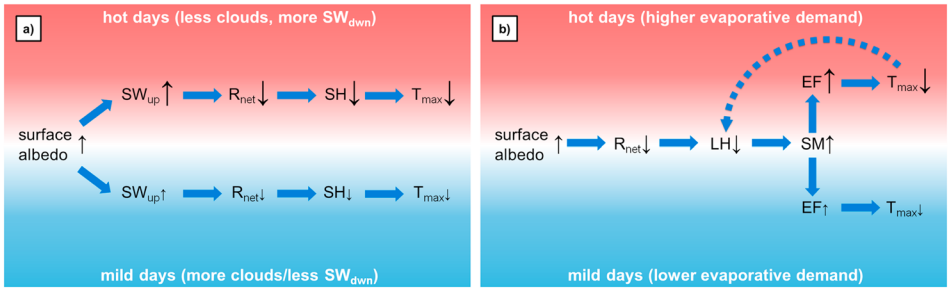

Figure 5. Conceptual diagram of the mechanisms leading to a preferential cooling of hot extremes. (a) In northern, radiation-limited ET regions the main mechanism is through an asymmetric radiative forcing effect linked to lower cloudiness during hotter days. (b) In southern, soil moisture-limited ET regions the main mechanism is through a feedback involving soil moisture. In this later case, an overall increase in soil moisture leads to a greater increase in evaporative fraction under hot conditions with higher evaporative demand. Note that the interactions shown here are not exhaustive, and only the mechanisms contributing to a preferential cooling of hot extremes compared to the mean are displayed. Black arrows represent anomalies relative to the control simulation. SWup: upwelling shortwave radiation; Rnet: net absorbed radiation; SH: sensible heat flux; LH: latent heat flux (or evapotranspiration); SM: total soil moisture; EF: evaporative fraction, Tmax: maximum daily temperature.

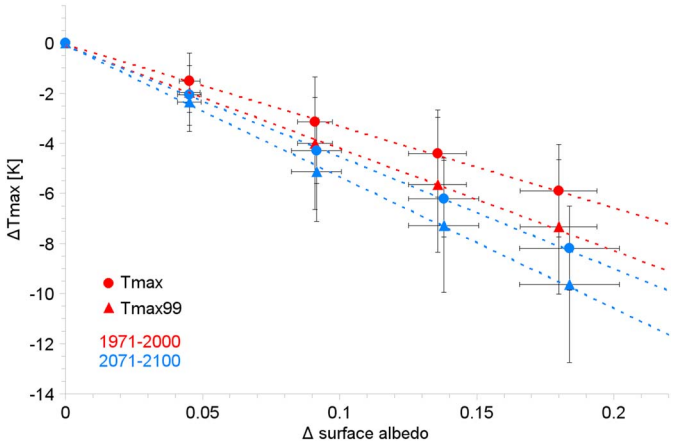

Figure 6. Summer (JJA) change (EXP minus CTL) in Tmax and Tmax99 (99th percentile of Tmax) as a function of the applied surface albedo increase for the periods 1971–2000 (red) and 2071–2100 (blue). Only grid points with vegetation cover of 60% or greater that are north of 30°N are considered. Error bars indicate the standard deviation of anomalies calculated across all considered grid points. The R^2 values of all linear regressions are greater or equal to 0.998.

3.3. Effects of Limited Spatial and Temporal Implementation

We investigate the extent to which the effect of land albedo management may be altered by limiting the modification of surface albedo to only croplands (instead of all vegetated areas) and over only summer months (July and August, instead of yearlong modifications). Indeed, a number of possible land albedo modification strategies are likely to be restricted to agricultural areas and to specific seasons (e.g., after crop harvest in the case of no-till agriculture [D14]).

The effect of limiting the albedo perturbation to croplands is summarized in Table 2. Overall, a weaker decrease in Tmax is found in EXP10c relative to EXP10 over croplands. Interestingly, the magnitude of the decrease in Tmax90 is less dampened than the mean Tmax, resulting in an increased asymmetry between the mean response and the effect for hot days. Applying the surface albedo perturbation exclusively over croplands reduces the cooling intensity over cropland. This in turn induces a weaker cloud cover feedback and subsequently a weaker decrease in SWnet, which would otherwise dampen the asymmetry, as discussed in section 3.2.1. Limiting the surface albedo perturbation further to only summer months (EXP10cJA) shows a further weakening of the summer cooling signal. This suggests that there is a significant carry over effect (from other seasons to summer) contributing to the summer cooling. This effect can be in part related to a weaker accumulation of soil moisture relative to CTL (see previous section); although other processes such as sea ice and ocean feedbacks might contribute to the carry over effect [*Davin and de Noblet-Ducoudré*, 2010]. Cooling magnitudes over the European continent are in general agreement with those found in the albedo-only experiment by D14, though with a weaker negative cloud feedback during cold days. Note that D14 additionally investigated the effects of increased resistance to soil evaporation imposed by the crop residue layer under conservation tillage. This would likely lead to larger overall SM savings, with less evaporative cooling in average summer days but more cooling in extreme hot days.

3.4. Climate Change and Linear Scaling of Preferential Cooling

A very strong linear scaling of the Tmax cooling as a function of the intensity of albedo increase is found in our experiments (Figure 6). This is in agreement with other studies related to surface albedo climate engineering [*Doughty et al.*, 2011; *Singarayer and Davies-Barnard*, 2012]. The preferential cooling during the warmest days (99th percentile of Tmax, Tmax99 in Figure 6) remains, as stronger surface albedo increase is applied. The linear scaling of the Tmax signal relative to the increase in surface albedo continues to hold under the future scenario (RCP8.5). However, the cooling intensity depends on the background climate. Indeed, for a given albedo increase, the resulting cooling is stronger under a future warmer climate.

This can be explained by a change in SM regime under a warmer future climate. Under the future scenario, SM decreases in CEU within the CTL simulation (Figure 7). This leads to a northward extension of the area where ET is SM-limited (consistent with analyses showing a long-term decrease of background soil moisture in climate change projections, e.g., *Wang* [2005], *Orlowsky and Seneviratne* [2012], and *Seneviratne et al.* [2013]). On the other hand, these drying trends are partly neutralized in EXP10 within the area of increased surface albedo (Figure 7). Therefore, the increase in surface albedo tends to limit the shift toward an SM-limited regime over this region in JJA. Hence, the contribution of the SM temperature feedback to the preferential cooling intensifies with time over regions with projected drying trends in CESM.

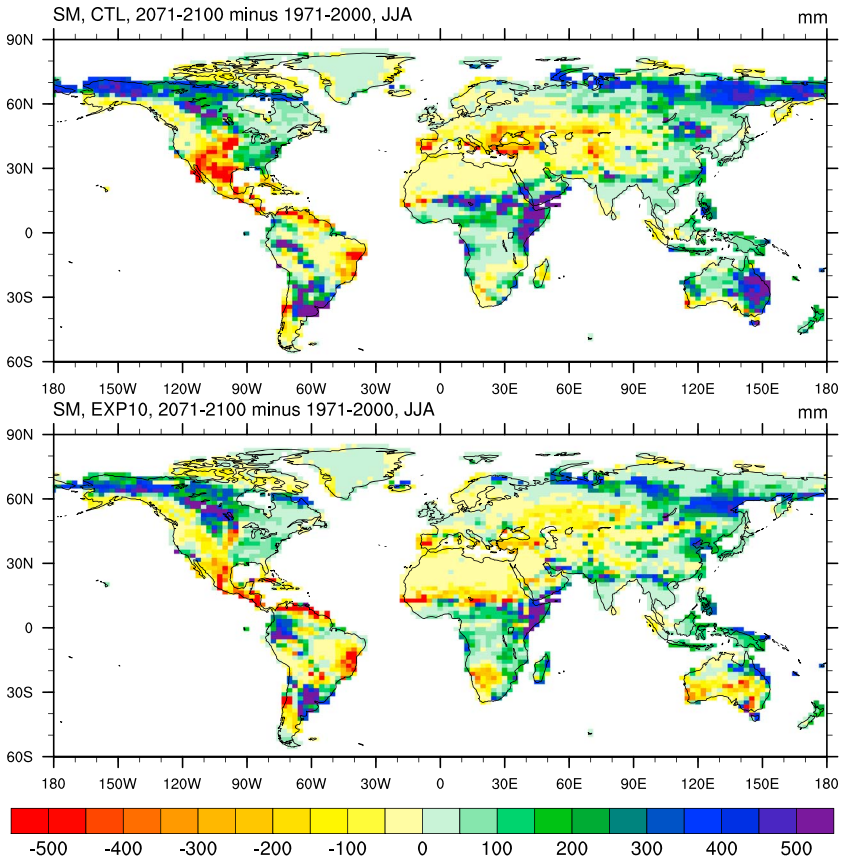

Figure 7. Summer (JJA) change (2071–2100 minus 1971–2000) in total SM (soil moisture) in (top) CTL and (bottom) EXP10.

A second mechanism contributing to the stronger efficacy of albedo change in a future climate is related to changes in cloud cover under higher CO_2 concentrations. CESM projects a distinct decrease in middle- and low-level cloud cover at midlatitudes in part due to increased planetary boundary layer stability, which reduces shallow convection, as well as to a poleward shift in storm tracks [*Colman and Hanson*, 2012; *Zelinka et al*., 2013]. Therefore, a given surface albedo increase has a greater effect on the planetary albedo owing to the larger amount of incoming radiation reaching the surface under lower cloud cover.

Since the intensity of the albedo-induced forcing is dependent on background cloud cover, it must be noted that the cloud cover response to climate change is a major source of uncertainty in climate projections [*Stevens and Bony*, 2013; *Boucher et al*., 2013]. Nonetheless, CESM was not found to be an outlier in terms of the shortwave cloud response to climate change in recent model intercomparison modeling experiments such as CMIP5 [*Vial et al*., 2013]. In addition, decreasing cloud cover over CEU seems to be robust within most of the CMIP5 models [*Boucher et al*., 2013]. In contrast, the case is not as clear over CNA as many models show conflicting signs of change in their cloud cover projections [*Boucher et al*., 2013].

3.5. Efficacy of Hot Extremes Mitigation

Comparing the RCP8.5 end of the 21st century and the historical late 20th century climatologies in CTL (Figure 8), CESM projects a prominent shift to warmer summer temperatures in response to anthropogenic forcings. Projected mean summer Tmax over CEU shows an increase of roughly 6.5 K in CTL. However, there is greater increase of summer Tmax90 by approximately 7.7 K. Under the climatic conditions at the end of the twentieth century, the intermediate experiment EXP10 negates a substantial portion of this anthropogenic perturbation in particular for the hottest days (mean Tmax: −3.6 K; Tmax90: −5.7 K over CEU). This information can be summarized with a measure of the cooling efficacy for different parts of the Tmax distribution (dividing the Tmax cooling from surface albedo engineering by the future anthropogenic warming). The high cooling efficacy in Tmax90 over CNA is limited in extent to a small area

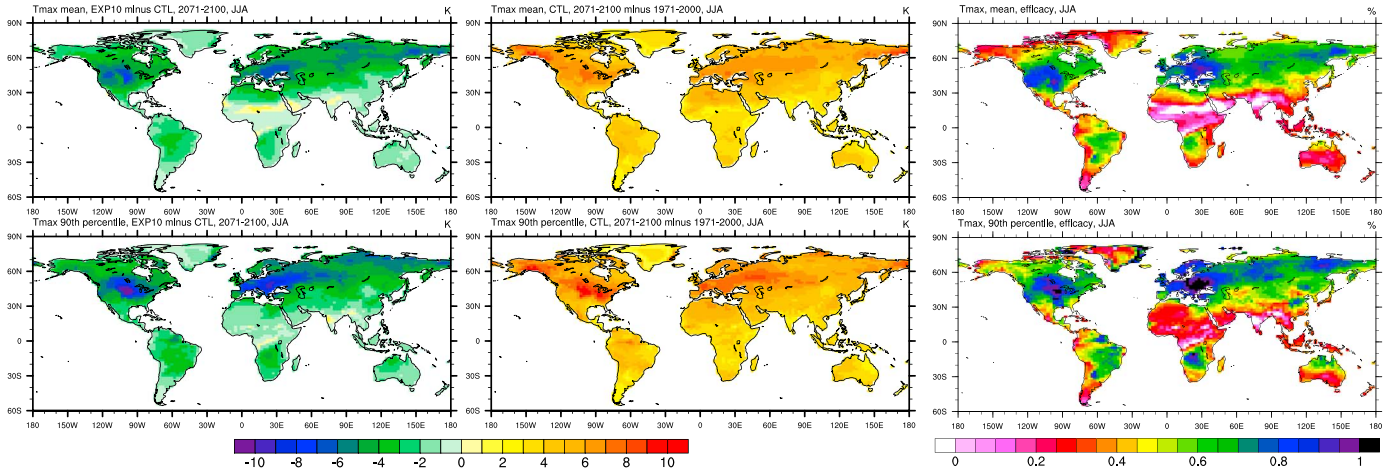

Figure 8. Comparison of change in (left) Tmax (EXP10 minus CTL) over the period 2071–2100 to (middle) projected climate change signal in Tmax within CTL and (right) the former divided by the latter multiplied by 100 giving the cooling efficacy. (top) Mean Tmax and (bottom) the 90th percentile of Tmax during summer (JJA).

west of the Great Lakes, while over CEU it is confined to the Eastern Europe for all experiments; in both regions negating the climate change signal entirely.

4. Summary and Conclusions

Historical and RCP8.5 experiments were performed in which the surface albedo over snow-free vegetated grid points was increased by 5, 10, 15, and 20%. All experiments show decreases in Tmax over midlatitude regions in the Southern and Northern Hemispheres during their respective summer seasons. The simulations also show a strong preferential cooling of hot extremes throughout the Northern midlatitudes during boreal summer in both the late 20th and the late 21st century conditions and a reduction of midlatitude soil drying.

The strongest preferential cooling is found over grasslands in the northwest of the Black Sea and the central United States, where enhanced SM-induced evaporative cooling (due to less overall SM depletion in the enhanced albedo simulation) is the largest contributor to this effect relative to CTL. But in non-soil moisture-limited, higher latitudes (e.g., Northern Europe) the identified preferential cooling of hot extremes is rather dominated by another mechanism, namely, the asymmetric radiative forcing of SWup (greatest during hot days when SWdwn is large). We note that the relative contribution of these two mechanisms depends on the temporal extent of the applied surface albedo forcing in the simulations (i.e., two summer months versus yearlong): The radiative mechanism is dominant in these regions when the albedo modification is only applied over a shorter summer period (similar to D14) but is overpowered by the SM feedback effect in simulations with yearlong albedo modifications. The latter effect also implies a reduction of summer drought conditions in these regions. It must be noted that the contribution of the SM temperature feedback is not explicitly quantified in our study, as an additional experiment, prescribing SM from CTL while perturbing the surface albedo similar to those performed within the Global Land-Atmosphere Coupling Experiment-CMIP5 experiment [*Seneviratne et al*., 2013], would be required. Such an experiment, however, lies beyond the scope of this study.

The magnitude of the preferential cooling is found to intensify over the regions of focus under late 21st century conditions despite near-constant surface albedo increase. This can be partially attributed to an increase in the albedo-induced radiative forcing due to negative trends in cloud cover under elevated CO_2 levels. In addition, the contribution of SM-ET cooling over a larger spatial extent intensifies the preferential cooling response.

In conclusion, we identify that global-scale changes in surface albedo over vegetated areas could substantially affect mean and, in particular, extreme hot temperatures over land in both present-day and future climate conditions. Although we note the hypothetical nature of the conducted simulations given the large geographical extent of the applied surface albedo change, these results could have important implications for climate engineering scenarios provided that further (ethical and practical) considerations are taken into account.

Acknowledgments
We sincerely thank Urs Beyerle and the team of the ETHZ Brutus Cluster for support with the computation of the simulations. Partial support of the ERC DROUGHT-HEAT project is acknowledged. Data used to generate figures, graphs, plots, and tables can be made available upon request to the corresponding author by email at micah.wilhelm@env.ethz.ch.

References

Alexander, L. V., X. Zhang, T. C. Peterson, J. Caesar, B. Gleason, A. M. G. Klein Tank, and J. L. Vazquez-Aguirre (2006), Global observed changes in daily climate extremes of temperature and precipitation, *J. Geophys. Res.*, *111*, D05109, doi:10.1029/2005JD006290.

Bellassen, V., and S. Luyssaert (2014), Increasing both forest stocks and timber harvest will buy time while we learn more about how trees absorb carbon, *Nature*, *506*, 153–155, doi:10.1038/506153a.

Boucher, O., et al. (2013), Clouds and aerosols, in *Climate Change 2013: The Physical Science Basis. Contribution of Working Group I to the Fifth Assessment Report of the Intergovernmental Panel on Climate Change*, edited by T. F. Stocker et al., Cambridge Univ. Press, Cambridge, U. K., and New York.

Colman, R. A., and L. I. Hanson (2012), On atmospheric radiative feedbacks associated with climate variability and change, *Clim. Dyn.*, *40*, 475–492, doi:10.1007/s00382-012-1391-3.

Curry, C. L., et al. (2014), A multimodel examination of climate extremes in an idealized geoengineering experiment, *J. Geophys. Res. Atmos.*, *119*, 3900–3923, doi:10.1002/2013JD020648.

Davin, E. L., and N. de Noblet-Ducoudré (2010), Climatic impact of global-scale deforestation: Radiative versus non-radiative processes, *J. Clim.*, *23*, 97–112, doi:10.1175/2009JCLI3102.1.

Davin, E. L., S. I. Seneviratne, P. Ciais, A. Olioso, and T. Wang (2014), Preferential cooling of hot extremes from cropland albedo management, *Proc. Natl. Acad. Sci. U.S.A.*, doi:10.1073/pnas.1317323111.

Donat, M. G., L. V. Alexander, H. Yang, I. Durre, R. Vose, and J. Caesar (2013), Global land-based datasets for monitoring climatic extremes, *Bull. Am. Meteorol. Soc.*, *4*, 997–1006, doi:10.1175/BAMS-D-12-00109.1.

Doughty, C. E., C. B. Field, and A. M. S. McMillan (2011), Can crop albedo be increased through the modification of leaf trichomes, and could this cool regional climate?, *Clim. Change*, *104*, 379–387, doi:10.1007/s10584-010-9936-0.

Fischer, E. M., S. I. Seneviratne, D. Lüthi, and C. Schär (2007), The contribution of land-atmosphere coupling to recent European summer heat waves, *Geophys. Res. Lett.*, *34*, L06707, doi:10.1029/2006GL029068.

Foley, J. A., et al. (2005), Global consequences of land use, *Science*, *309*(5734), 570–574, doi:10.1126/science.1111772.

Friedlingstein, P., et al. (2014), Persistent growth of CO_2 emissions and implications for reaching climate targets, *Nat. Geosci.*, *7*(10), 709–715, doi:10.1038/ngeo2248.

Gent, P. R., et al. (2011), The community climate system model version 4, *J. Clim.*, *24*, 4973–4991, doi:10.1175/2011JCLI4083.1.

Goldewijk, K. K. (2001), Estimating global land use change over the past 300 years: The HYDE database, *Global Biogeochem. Cycles*, *15*, 417–433, doi:10.1029/1999GB001232.

Guillod, B. P., et al. (2014), Land-surface controls on afternoon precipitation diagnosed from observational data: Uncertainties and confounding factors, *Atmos. Chem. Phys.*, *14*(16), 8343–8367, doi:10.5194/acp-14-8343-2014.

Hirschi, M., S. I. Seneviratne, V. Alexandrov, F. Boberg, C. Boroneant, O. B. Christensen, H. Formayer, B. Orlowsky, and P. Stepanek (2011), Observational evidence for soil-moisture impact on hot extremes in southeastern Europe, *Nat. Geosci.*, *4*, 17–21, doi:10.1038/ngeo1032.

Intergovernmental Panel on Climate Change (IPCC) (2012), *Managing the Risks of Extreme Events and Disasters to Advance Climate Change Adaptation. A Special Report of Working Groups I and II of the Intergovernmental Panel on Climate Change*, edited by C.B. Field et al., 582 pp., Cambridge Univ. Press, Cambridge, U. K., and New York.

Intergovernmental Panel on Climate Change (IPCC) (2013), *Climate Change 2013: The Physical Science Basis. Contribution of Working Group I to the Fifth Assessment Report of the Intergovernmental Panel on Climate Change*, edited by T. F. Stocker et al., 1535 pp., Cambridge Univ. Press, Cambridge, U. K., and New York.

Irvine, P. J., A. Ridgwell, and D. J. Lunt (2011), Climatic effects of surface albedo geoengineering, *J. Geophys. Res.*, *116*, D24112, doi:10.1029/2011JD016281.

Koster, R. D., et al. (2004), Regions of strong coupling between soil moisture and precipitation, *Science*, *305*(5687), 1138–1140, doi:10.1126/science.1100217.

Koster, R. D., et al. (2006), GLACE: The Global Land–Atmosphere Coupling Experiment. Part I: Overview, *J. Hydrometeorol.*, *7*, 590–610, doi:10.1175/JHM510.1.

Koster, R. D., et al. (2010), The contribution of land initialization to subseasonal forecast skill: First results from the GLACE-2 project, *Geophys. Res. Lett*, *37*, L02402, doi:10.1029/2009GL041677.

Lenton, T. M., and N. E. Vaughan (2009), The radiative forcing potential of different climate geoengineering options, *Atmos. Chem. Phys.*, *9*, 5539–5561, doi:10.5194/acp-9-5539-2009.

Lobell, D. B., G. Bala, and P. B. Duffy (2006), Biogeophysical impacts of cropland management changes on climate, *Geophys. Res. Lett.*, *33*, L06708, doi:10.1029/2005GL025492.

Luyssaert, S., et al. (2014), Land management and land-cover change have impacts of similar magnitude on surface temperature, *Nat. Clim. Change*, *4*, 389–393, doi:10.1038/nclimate2196.

Miralles, D. G., A. J. Teuling, C. C. van Heerwaarden, and J. Vila-Guerau de Arellano (2014), Mega-heatwave temperatures due to combined soil desiccation and atmospheric heat accumulation, *Nat. Geosci.*, *7*(5), 345–349, doi:10.1038/NGEO2141.

Mueller, B., and S. I. Seneviratne (2012), Hot days induced by precipitation deficits at the global scale, *Proc. Natl. Acad. Sci. U.S.A.*, *109*, 12,398–12,403.

Oleson, K. W., G. B. Bonan, and J. Feddema (2010), Effects of white roofs on urban temperature in a global climate model, *Geophys. Res. Lett.*, *37*, L03701, doi:10.1029/2009GL042194.

Orlowsky, B., and S. I. Seneviratne (2012), Global changes in extreme events: Regional and seasonal dimension, *Clim. Change*, *110*, 669–696, doi:10.1007/s10584-011-0122-9.

Orlowsky, B., and S.I. Seneviratne (2013), Elusive drought: Uncertainty in observed trends and short- and long-term CMIP5 projections, *Hydrol. Earth Syst. Sci.*, *17*, 1765–1781, doi:10.5194/hess-17-1765-2013.

Ramankutty, N., A. T. Evan, C. Monfreda, and J. A. Foley (2008), Farming the planet: 1. Geographic distribution of global agricultural lands in the year 2000, *Global Biogeochem. Cycles*, *22*, GB1003, doi:10.1029/2007GB002952.

Ridgwell, A., J. S. Singarayer, A. M. Hetherington, and P. J. Valdes (2009), Tackling regional climate change by leaf albedo bio-geoengineering, *Curr. Biol.*, *19*, 146–150, doi:10.1016/j.cub.2008.12.025.

Seneviratne, S. I., D. Lüthi, M. Litschi, and C. Schär (2006), Land-atmosphere coupling and climate change in Europe, *Nature*, *443*, 205–209, doi:10.1038/nature05095.

Seneviratne, S. I., T. Corti, E. L. Davin, M. Hirschi, E. B. Jaeger, I. Lehner, B. Orlowsky, and A. J. Teuling (2010), Investigating soil moisture-climate interactions in a changing climate: A review, *Earth Sci. Rev.*, *99*(3–4), 125–161, doi:10.1016/j.earscirev.2010.02.004.

Seneviratne, S. I., et al. (2012), Changes in climate extremes and their impacts on the natural physical environment, in *Managing the Risks of Extreme Events and Disasters to Advance Climate Change Adaptation. A Special Report of Working Groups I and II of the Intergovernmental Panel on Climate Change*, edited by C. B. Field et al., pp. 109–230, Cambridge Univ. Press, Cambridge, New York.

Seneviratne, S. I., et al. (2013), Impact of soil moisture-climate feedbacks on CMIP5 projections: First results from the GLACE-CMIP5 experiment, *Geophys. Res. Lett.*, *40*, 5212–5217, doi:10.1002/grl.50956.

Seneviratne, S. I., M. Donat, B. Mueller, and L. V. Alexander (2014), No pause in the increase of hot temperature extremes, *Nat. Clim. Change*, *4*, 161–163, doi:10.1007/s10584-006-9051-4.

Shepherd, J. G., and Working Group on Geoengineering the Climate (2009), *Geoengineering the Climate: Science, Governance and Uncertainty*, 98 pp., Royal Soc., London, U. K.

Sillmann, J., V. V. Kharin, F. W. Zwiers, X. Zhang, and D. Bronaugh (2013), Climate extremes indices in the CMIP5 multimodel ensemble: Part 2. Future climate projections, *J. Geophys. Res. Atmos.*, *118*, 2473–2493, doi:10.1002/jgrd.50188.

Singarayer, J. S., and T. Davies-Barnard (2012), Regional climate change mitigation with crops: Context and assessment, *Philos. Trans. R. Soc. London, Ser. A*, *370*, 4301–4316, doi:10.1098/rsta.2012.0010.

Solomon, S., G.-K. Plattner, R. Knutti, and P. Friedlingstein (2009), Irreversible climate change due to carbon dioxide emissions, *Proc. Natl. Acad. Sci. U.S.A.*, *106*, 1704–1709, doi:10.1073/pnas.0812721106.

Stevens, B., and S. Bony (2013), What are climate models missing?, *Science*, *340*(6136), 1053–1054, doi:10.1126/science.1237554.

Taylor, C. M., R. A. de Jeu, F. Guichard, P. P. Harris, and W. A. Dorigo (2012a), Afternoon rain more likely over drier soils, *Nature*, *489*(7416), 423–426, doi:10.1038/nature11377.

Taylor, K. E., R. J. Stouffer, and G. A. Meehl (2012b), An overview of CMIP5 and the experiment design, *Bull. Am. Meteorol. Soc.*, *93*, 485–498, doi:10.1175/BAMS-D-11-00094.1.

Tebaldi, C., K. Hayhoe, J. M. Arblaster, and G. A. Meehl (2006), Going to the extremes, *Clim. Change*, *79*(3–4), 185–211, doi:10.1007/s10584-006-9051-4.

Teuling, A. J., et al. (2009), A regional perspective on trends in continental evaporation, *Geophys. Res. Lett.*, *36*, L02404, doi:10.1029/2008GL036584.

Vaughan, N. E., and T. M. Lenton (2011), A review of climate geoengineering proposals, *Clim. Change*, *109*, 745–790, doi:10.1007/s10584-011-0027-7.

Vial, J., J. L. Defresne, and S. Bony (2013), On the interpretation of inter-model spread in CMIP5 climate sensitivity estimates, *Clim. Dyn.*, *41*(11–12), 3339–3362, doi:10.1007/s00382-013-1725-9.

Wang, G. (2005), Agricultural drought in a future climate: Results from 15 global climate models participating in the IPCC 4th assessment, *Clim. Dyn.*, *25*, 739–753, doi:10.1007/s00382-005-0057-9.

Weaver, A. J., K. Zickfeld, A. Montenegro, and M. Eby (2007), Long term climate implications of 2050 emission reduction targets, *Geophys. Res. Lett.*, *34*, L19703, doi:10.1029/2007GL031018.

Wigley, T. M. (2006), A combined mitigation/geoengineering approach to climate stabilization, *Science*, *314*(5798), 452–454, doi:10.1126/science.1131728.

Zelinka, M. D., S. A. Klein, K. E. Taylor, T. Andrews, M. J. Webb, J. M. Gregory, and P. M. Forster (2013), Contributions of different cloud types to feedbacks and rapid adjustments in CMIP5, *J. Clim.*, *26*, 5007–5027, doi:10.1175/JCLI-D-12-00555.1.